

Tuning anisotropy by impurities: magnetocaloric experiments on $\text{CsNi}_{0.9}\text{Fe}_{0.1}\text{Cl}_3$

 J. Wolf^{1,a}, K. Kiefer¹, M.C. Rheinstädter^{1,b}, K. Knorr¹, and M. Enderle^{1,2,3}
¹ Technische Physik, Bau 38, Universität des Saarlandes, 66123 Saarbrücken, Germany

² Condensed Matter Physics and Chemistry, Risø National Laboratory, 4000 Roskilde, Denmark

³ Institut Laue-Langevin, BP 156, 38042 Grenoble Cedex 9, France

Received 20 April 2001

Abstract. The magnetic phase diagram of the Fe^{2+} doped hexagonal ABX_3 compound $\text{CsNi}_{0.9}\text{Fe}_{0.1}\text{Cl}_3$ is investigated by heat capacity and magnetocaloric experiments. In spite of the high doping concentration, some phase boundaries appear surprisingly well-defined, while others are broadened significantly. The discussion of this behaviour clarifies the potentials and limitations of doping as a means to manipulate the effective anisotropy in quasi one-dimensional ABX_3 compounds.

PACS. 75.30.Sg Magnetocaloric effect, magnetic cooling – 75.30.Kz Magnetic phase boundaries

1 Introduction

Hexagonal ABX_3 compounds have been studied intensely both with respect to quasi one-dimensional properties and with respect to frustrated antiferromagnetic interactions on a triangular lattice. In these compounds A stands for an alkali ion, B is a divalent transition metal ion and carries the localized magnetic moment, and X is a halogen ion. The magnetic B ions are strongly coupled along the hexagonal c -direction by three equivalent superexchange paths each involving one halogen ion. The superexchange paths in the hexagonal ab -plane involve two halogen ions and are weaker by at least one order of magnitude. The magnetic behaviour is usually modeled by the Hamiltonian

$$\mathcal{H} = 2J \sum_i^{\text{intra}} \mathbf{S}_i \mathbf{S}_{i+1} + 2J' \sum_{i \neq j}^{\text{inter}} \mathbf{S}_i \mathbf{S}_j + D \sum_i (S_i^z)^2 - g\mu_B \mathbf{H} \sum_i \mathbf{S}_i \quad (1)$$

where $2J$ denotes the exchange per bond along the chain direction c , $2J'$ the effective interchain exchange per bond in the ab -plane, D the uniaxial single-ion crystal-field anisotropy and $\mathbf{H} = \mathbf{B}/\mu_0$ the applied magnetic field. The sign of D determines the preferred direction of the spins relative to the crystal axes. For $D < 0$ the anisotropy energy is minimized with the spins along the $z(c)$ -direction (Ising anisotropy), for $D > 0$ the spins prefer an alignment in the ab -plane (easy-plane anisotropy). Due to

the frustrated antiferromagnetic interchain interaction J' , the topology of the B - T phase diagram depends sensitively on D . Upon variation of D , at least six different types of B - T diagrams are expected, for strong and weak Ising anisotropy, Heisenberg behaviour, weak, medium and strong easy-plane anisotropy. Most of these are realized by one or the other ABX_3 compound [1].

Doping of weakly anisotropic compounds with another magnetic ion has been proposed as a means to modify the anisotropy in a controlled way [2]. Here we investigate Fe^{2+} -doped CsNiCl_3 , where the strong easy-plane type single-ion anisotropy of the Fe^{2+} competes with the weak Ising anisotropy of the Ni^{2+} . CsNiCl_3 has antiferromagnetic exchange $J > 0$ along the hexagonal axis, CsFeCl_3 ferromagnetic $J < 0$. In both compounds the interchain interaction is antiferromagnetic, $J' > 0$.

If there was no single-ion anisotropy D , the low-temperature phase of CsNiCl_3 would be a six-sublattice antiferromagnetic structure, where the spins within one chain order antiparallel, and the magnetic moment on a triangle in the ab -plane is cancelled with neighbouring spins including an angle of 120° (helix phase H). Due to the weak Ising anisotropy of CsNiCl_3 , the spins order parallel to an ac -plane and the angle between adjacent spins in the ab -plane slightly deviates from 120° . This distorted helix structure is also abbreviated H. Two phase transitions in zero magnetic field are observed, paramagnetic-intermediate (P-I) and intermediate-distorted helix (I-H), corresponding to the onset of long-range order of the spin components parallel (P-I) and perpendicular to c (I-H). With a field applied along the c -axis, the Ising anisotropy is effectively reduced and finally cancelled at the spin-flop transition, where the spins flip to a 120° -structure in the ab -plane, with a uniform tilt towards the magnetic field.

^a Present address: Agilent Technologies, 1400 Fountaingrove Pkwy, Santa Rosa, CA 95403, USA

^b e-mail: maikel@mx.uni-saarland.de

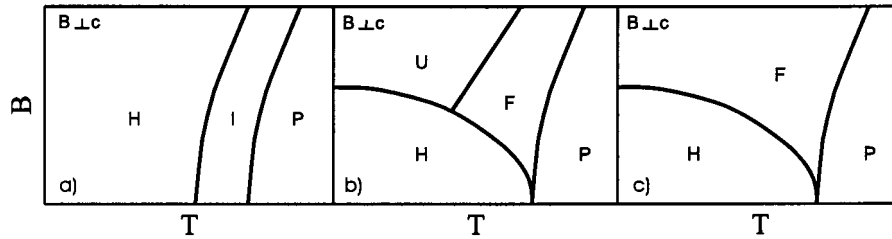


Fig. 1. Schematic phase diagrams of stacked triangular antiferromagnets with different single-ion anisotropies and magnetic field $B = \mu_0 H \perp c$. a) Weak Ising anisotropy $D < 0$. b) Weak easy-plane anisotropy $0 < D/3J' < 1$. c) Medium easy-plane anisotropy $D/3J' > 1$. With large easy-plane anisotropy (D large compared to J, J'), there is no ordered phase for this field direction. H: distorted helix phase, I: intermediate phase, P: paramagnetic phase, U: umbrella phase, F: fan phase, *cf.* text.

With the field perpendicular to c , there are always two phase transitions. Figure 1a displays this type of phase diagram schematically.

The *very large* easy-plane single-ion anisotropy of CsFeCl_3 leads to suppression of long-range order at zero field. Above a critical field B_c along the symmetry axis c , a transition into a long-range ordered phase is observed, while for $B \perp c$ no ordering can be found.

Antiferromagnets with a *medium* easy-plane anisotropy as CsMnBr_3 have one single phase transition P-H into a 120° -structure H at both zero field and fields applied parallel to the symmetry axis. With a magnetic field in the easy plane ($B \perp c$), the easy-plane anisotropy prevents an easy alignment of the 120° -structure perpendicular to the magnetic field, and an intermediate fan phase F emerges (Fig. 1c). In the F phase, the easy-plane anisotropy D effectively overcomes the antiferromagnetic interchain interaction J' , so that all spins remain in the easy plane. Two spins on a triangle become parallel, the third antiparallel (apart from a small canting of all spins towards the applied field). At lower temperatures, with $B \perp c$, a distorted helix structure H is entered.

With *weak* easy-plane anisotropy, $0 < D/3J' < 1$, there is one single phase transition for $B \parallel c$ as in the medium anisotropy case. However, three ordered magnetic phases are predicted for $B \perp c$ [3–5] (Fig. 1b). At low magnetic fields, the H phase is reached through an intermediate phase F as with medium easy-plane anisotropy. Beyond a critical field, however, the low-temperature structure is a so-called umbrella phase U. Here the spins on a triangle orient almost perpendicular to the magnetic field with one spin in the easy-plane, while the two other spins include an angle with the easy-plane. This resembles a distorted 120° structure perpendicular to the easy plane, which satisfies the interchain exchange better than the fan structure and therefore is the stable phase at larger values of the order parameter. The tilt angle of two spins on a triangle out of the easy plane depends on the ratio D/J' and so does the U-F transition temperature. This case of weak easy-plane anisotropy has not been observed on pure ABX_3 compounds. However, the phase diagram of $\text{CsNi}_{0.98}\text{Fe}_{0.02}\text{Cl}_3$ with $B \perp c$ displays the topology of the weak easy anisotropy case [6, 7], with three magnetic

phases, markedly different from the medium anisotropy case realized by CsMnBr_3 .

In spite of the frustrated interchain interactions and the doping, the phase transitions observed on $\text{CsNi}_{0.98}\text{Fe}_{0.02}\text{Cl}_3$ are rather well-developed and only the field-dependent transition H-U displays some broadening [6]. Here we present an investigation of the compound with five times larger doping, $\text{CsNi}_{0.9}\text{Fe}_{0.1}\text{Cl}_3$, by specific heat capacity and ac magnetocaloric techniques with the magnetic field applied perpendicular to c . The two methods can be applied with the same experimental equipment. Their combination turns out to be an effective tool for the exploration of phase diagrams. It is the aim of this study to investigate how far the tuning of the anisotropy can be driven by a five times larger doping with Fe^{2+} . As $0.034 < D/3J' < 0.23$ was found for the 2% doped sample [6], the ratio $D/3J'$ of the 10% compound might already exceed the critical value of 1, thus leading to a phase diagram of the medium-anisotropy case as in CsMnBr_3 . On the other hand, the higher doped sample might show more pronounced traces of disorder, up to the complete destruction of phase transitions.

Our experiments of the 10% sample reveal a phase diagram very similar to the 2% compound, with the general topology of the weak-anisotropy case. However, we observe several surprising qualitative differences. The discussion of these differences leads to a microscopic model which not only explains consistently all observed features, but also illuminates the potentials and limitations of doping as a means to control the anisotropy in ABX_3 compounds.

2 Experimental

The experimental setup for the calorimetric measurements consists of a sapphire sample holder of dimension $10 \times 10 \times 0.2 \text{ mm}^3$ which is suspended from four nylon-filaments in a copper frame. The temperature of the copper frame can be controlled to $\Delta T/T = 10^{-5}$. One side of the sample holder carries a Cernox thin film thermometer and a sputtered Au heater. The sample is attached to the other side of the sapphire plate by Apiezon N grease. The thoroughly heatsunk electrical connections to heater and thermometer establish a (weak) thermal link to the copper frame which serves as an accurately controlled thermal bath. This arrangement is vacuum shielded and placed in

the VTI of a 12 T-cryomagnet. A detailed description of the apparatus can be found in [8]. Using this experimental setup both the specific heat capacity and the magnetocaloric measurements were performed.

For the specific heat capacity two different measurement processes were employed. The B - T phase diagram was determined by the very fast continuous cooling method [9]. For a quantitative analysis we used the quasi-adiabatic heat pulse method.

The investigated crystal of CsNi_{0.9}Fe_{0.1}Cl₃ had a mass of 38.34 mg.

The magnetocaloric effect θ_H (MCE) is defined as the adiabatic change of the temperature of a magnetized material upon variation of an external magnetic field ($H = B/\mu_0$).

$$\begin{aligned} \theta_H &\equiv \left. \frac{dT(H, S)}{dH} \right|_{S = \text{const.}} = - \left(\frac{\partial S}{\partial H} \right)_T \bigg/ \left(\frac{\partial S}{\partial T} \right)_H \\ &= - \frac{T}{C_H} \left(\frac{\partial M}{\partial T} \right)_H. \end{aligned} \quad (2)$$

As the specific heat capacity is always positive, the MCE changes sign with $\left(\frac{\partial M}{\partial T} \right)_H$. It is positive for a standard paramagnetic or ferromagnetic material where $\left(\frac{\partial M}{\partial T} \right)_H < 0$ and an increase of the magnetic field causes heating. It is negative for a simple antiferromagnet, where $\left(\frac{\partial M}{\partial T} \right)_H > 0$ and an increase of the magnetic field causes cooling. The MCE can be measured by sweeping a magnetic field and simultaneously detecting the temperature change of the sample. In order to assure adiabatic conditions, it is necessary to use a sufficiently fast sweep rate such that the temperature change cannot drain into the heat bath. However, due to numerous relaxation processes in the experimental setup it is difficult to accurately determine the MCE as a function of the sample temperature and magnetic field with this quasi-static method. This problem of temperature relaxation can be solved with the ac-method innovated by Fischer *et al.* [10]. In this dynamic technique a small sinusoidal modulation is added to the static external field B_0 ,

$$B_{\text{ext}}(t) = B_0 + \Delta B \sin(2\pi\nu t), \quad (3)$$

and the resulting periodic temperature change ΔT is detected

$$T(t) = T_0 + \Delta T \sin(2\pi\nu t + \phi). \quad (4)$$

The low thermal conductance between sample holder and heat bath and the small heat capacity of the sample holder assure a minimal attenuation of the magnetocaloric effect. For our setup, the modulation frequency of $\nu = 0.05$ Hz and the modulation amplitude of $\Delta B = 0.05$ T proved most appropriate. At higher frequencies, the amplitude of the temperature oscillations ΔT is dampened by internal relaxation (sample-sample holder relaxation and spin-lattice relaxation), at lower frequencies it is reduced by the sample-bath relaxation. The small observed phase shift ϕ between the periodically modulated magnetic field and

the temperature oscillations can be attributed to internal relaxation. ΔT was checked to be proportional to the magnetic field amplitude ΔB . The present choice of ΔB assures a reasonable signal-to-noise ratio while keeping the deviation from the applied field as small as possible. Too large deviations from B_0 may become problematic in the vicinity of a phase boundary where the MCE itself displays large changes with the magnetic field. It should be noted, that the quantity measured here, $\theta_H^* = \frac{\Delta T}{\Delta B}$, corresponds to the difference quotient, due to the finite rather than infinitesimal value of ΔB . In spite of the careful choice of ν and ΔB , the absolute value of θ_H^* is still affected by damping due to the heat capacity of the sample holder and the temperature sensor, as well as the relaxation processes mentioned above. Nonetheless, the measurement of relative changes of θ_H^* is perfectly suited to determine phase transitions. In particular, phase boundaries which are parallel to the temperature axis are easily detected, while they appear smeared out or are invisible in a specific heat capacity experiment.

Here we combine magnetocaloric and specific heat experiments to determine the phase diagram of CsNi_{0.9}Fe_{0.1}Cl₃. The experiments have been performed with the magnetic field applied in the ab -plane, within the cleavage plane. Assuming that the doped samples cleave in the same way as pure CsNiCl₃, the field is parallel to a crystallographic a -direction. With our experimental setup, the accurate orientation with respect to the magnetic field could not be controlled – however, the angle of the field within the ab -plane is expected to be entirely unimportant and slight deviations of the 90° angle between c -axis and magnetic field should not be crucial. We estimate that both angles are correct within a few degrees.

3 Results

Specific heat results obtained with the continuous cooling method at different magnetic fields are shown in Figure 2. The phase transition P-F from the paramagnetic into a first ordered phase is clearly visible and forms a pronounced anomaly which moves first to slightly lower and then to higher temperatures with increasing magnetic field. Towards the highest magnetic fields this anomaly sharpens significantly. Below the P-F anomaly, a second rather broad maximum is seen at low fields, moving to lower temperatures with increasing field and then vanishing. At higher fields, a broad maximum below the sharp phase transition anomaly is observed anew, moving towards higher temperature as the field increases. We identify the broad maximum at low fields with the F-H phase transition, that in the high-field region as the F-U transition. At zero field we observe a shoulder at the high-temperature wing of the main anomaly which develops into the sharp feature identified as the P-F transition at higher field. This shoulder is even better resolved in measurements with the quasi-adiabatic method, Figure 3. Hence the zero-field phase transition appears to be slightly split.

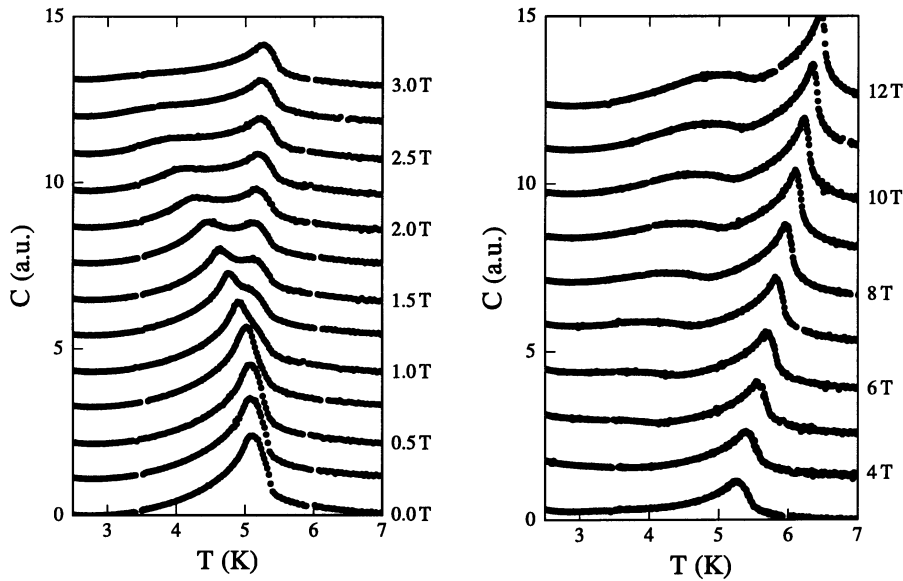


Fig. 2. Heat capacity of $\text{CsNi}_{0.9}\text{Fe}_{0.1}\text{Cl}_3$ at different magnetic fields $B \perp c$. The heat capacity is measured by the continuous cooling method and has arbitrary units. A polynomial fit to the zero field curve, excluding the critical region, was subtracted from the data. The left panel shows magnetic fields from 0 to 3 T, the right panel from 3 to 12 T. All curves are displaced vertically.

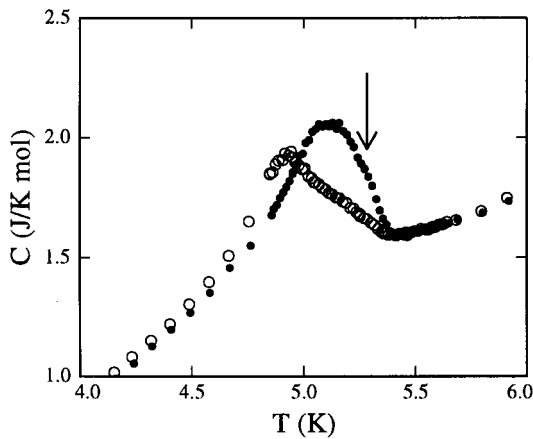


Fig. 3. Specific heat capacity of $\text{CsNi}_{0.9}\text{Fe}_{0.1}\text{Cl}_3$ at zero field (full circles) and 1 T (open circles), measured with the quasi-adiabatic method. The shoulder in the zero-field peak indicates a splitting of the zero-field transition.

The width and close separation of the phase transitions does not allow a systematic determination of the critical behaviour. We tried nevertheless to quantify the apparent narrowing of the P-F transition. A Gaussian distribution of transition temperatures convoluted with a power law divergence was fitted to the data at 3 T and 12 T. In spite of large error bars for the critical behaviour, the Gaussian width of the transition can be determined reliably, yielding $\sigma = 0.11 \pm 0.02$ K at 3 T and $\sigma = 0.04 \pm 0.01$ K at 12 T. A similar sharpening had been observed for the single phase transition of $\text{CsNi}_{0.98}\text{Fe}_{0.02}\text{Cl}_3$ with $B \parallel c$ [7].

Figure 4 displays an overview of the magnetocaloric effect *versus* magnetic field and temperature. Figure 5 col-

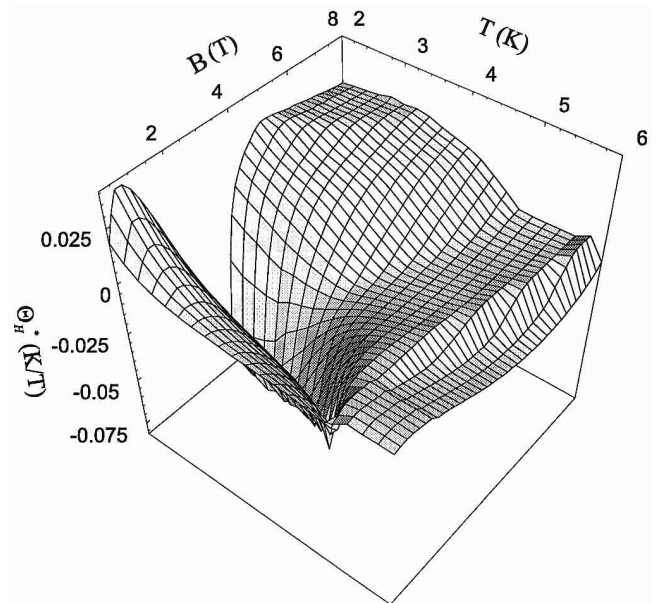


Fig. 4. 3D plot of θ_H^* for $\text{CsNi}_{0.9}\text{Fe}_{0.1}\text{Cl}_3$.

lects several field scans at representative temperatures. Figure 6 contains temperature scans at selected fields. In order to be able to assign phase transitions to the anomalies of the MCE, we collect distinct features from all three figures and compare them, where possible, to heat capacity results:

- i) A pronounced “canyon” is evident in Figure 4, visible as a minimum in the field scans of Figure 5. Figure 5 reveals, that upon increasing magnetic field across this canyon, a region of negative decreasing MCE is succeeded by an increase and a change of curvature

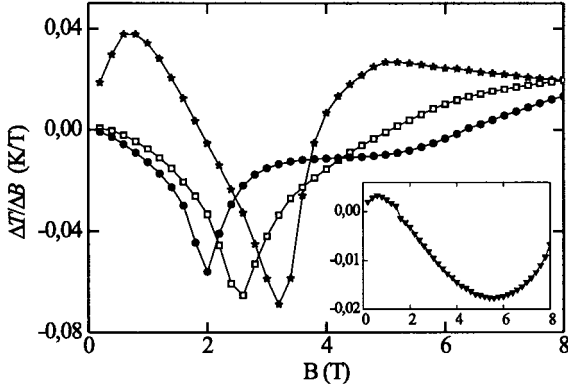


Fig. 5. Magnetocaloric effect of $\text{CsNi}_{0.9}\text{Fe}_{0.1}\text{Cl}_3$ versus the external magnetic field at 2.0 K (stars), 3.6 K (open squares), 4.2 K (full circles). The inset shows MCE at 6.0 K (open triangles).

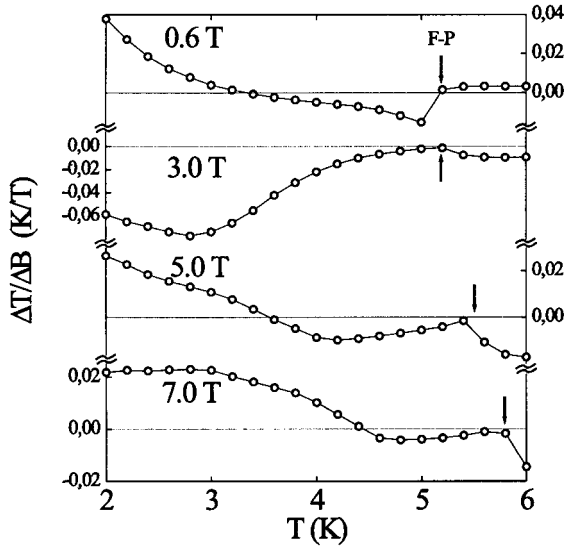


Fig. 6. Temperature dependence of the magnetocaloric effect of $\text{CsNi}_{0.9}\text{Fe}_{0.1}\text{Cl}_3$ at different magnetic fields. $\downarrow^{\text{F-P}}$ indicates the location of the specific heat maximum at the phase transition between paramagnetic and fan phase.

towards positive values of θ_H^* . This inflection point in the increasing slope can be followed from lowest temperatures up to about 5 K. It shifts towards lower magnetic fields at higher temperatures (Fig. 5) and coincides with the lower of the two maxima in the specific heat capacity at low fields, as long as the specific heat maximum can be followed. Therefore we attribute the inflection point of the MCE to the boundary of the H phase. This phase boundary turns out to be almost parallel to the temperature axis at low temperatures. This fact is at least partly responsible for the weak and broad appearance of the corresponding specific heat anomaly. The combination of field-dependent magnetocaloric effect and specific heat capacity experiments proves to be most effective for the determination of this phase boundary.

- ii) The large heat capacity anomaly which indicates the P-F phase boundary coincides with a clearly visible kink anomaly in the $\theta_H^*(H)$ curves in Figures 4 and 6. The specific heat anomaly at the P-F transition is marked by $\downarrow^{\text{F-P}}$ in the temperature dependent MCE-curves of Figure 6. There is no doubt that a conventional heat capacity experiment is best suited to determine a B - T phase boundary with such a steep slope. However, it is worth noting that the phase transition also leads to a clear feature in the temperature dependence of the MCE.
- iii) A flat plateau at high magnetic field strength and lowest temperatures (see Fig. 4) is followed by a wide descent towards higher temperatures. The descent ends in a “valley” parallel to the kink which indicates the P-F phase boundary. A thorough comparison of the second broad specific heat maximum at fields above 3 T, identified as the F-U transition, shows that the extension of the specific heat anomaly covers the wide descent of the MCE from the plateau towards the valley at higher temperatures. We interpret the broad features in both types of experiments as a far-flung broadening of the phase boundary between fan and umbrella phase. Again it is the specific heat capacity rather than a temperature dependent MCE experiment which reliably defines the onset of the F-U phase transition at higher magnetic fields, where the phase boundary is steep. However, the corresponding feature is located in the MCE measurements and can be traced along arbitrary $B(T)$ lines, into those regions of the B - T diagram where the specific heat capacity does not disclose the boundaries. The MCE in Figure 4 reveals that the F-U transition region surrounds the U phase between 3 T and 4 T. It also indicates the boundary of the transition region towards the pure U phase, identified as the plateau.

Some additional observations concern the sign of the MCE which is directly connected to the sign of $\partial M/\partial T$ through equation (2). We first review $\partial M/\partial T$ in related ABX_3 compounds. Close to the phase transition between paramagnetic and ordered phases, CsNiCl_3 [20] as well as $\text{CsNi}_{0.98}\text{Fe}_{0.02}\text{Cl}_3$ [19] and CsMnBr_3 [21] or CsVBr_3 [22] have a positive $\partial M/\partial T$ in the P phase, and hence the P phase is characterized by a negative θ_H close to the phase transition. This is a consequence of the one-dimensional antiferromagnetic short-range order in these compounds which is already well developed far above the phase transition. The H phase in CsMnBr_3 [21], CsVBr_3 , RbVBr_3 [22] has positive $\partial M/\partial T$. The F phase shows $\partial M/\partial T < 0$ in CsMnBr_3 , CsVBr_3 , RbVBr_3 [21,22], however, $\partial M/\partial T$ is again very small in the F phase of $\text{CsNi}_{0.98}\text{Fe}_{0.02}\text{Cl}_3$ [19]. It is not clear whether or not $\partial M/\partial T$ may even change sign in this phase. In the temperature region of the U phase, the magnetization slope $\partial M/\partial T < 0$ of $\text{CsNi}_{0.98}\text{Fe}_{0.02}\text{Cl}_3$ [19] is clearly negative, as in the structurally similar spin-flop phase in CsNiCl_3 . From the comparison with these related ABX_3 structures we may expect a negative θ_H^* in the P phase and a positive θ_H^* in the U phase of $\text{CsNi}_{0.9}\text{Fe}_{0.1}\text{Cl}_3$. In the H and F phases, θ_H^* is expected to be small.

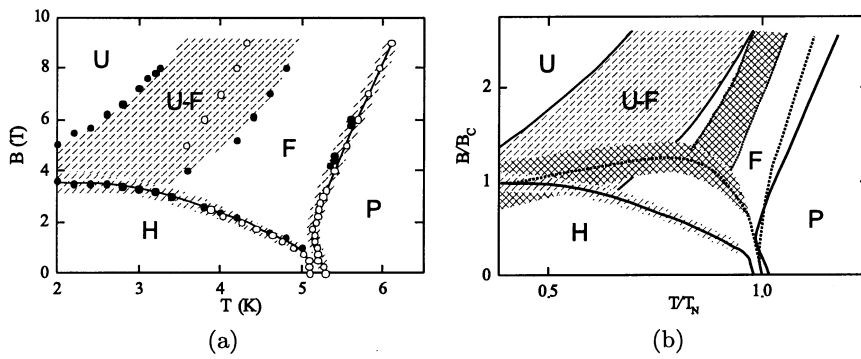


Fig. 7. (a) Phase diagram of $\text{CsNi}_{0.9}\text{Fe}_{0.1}\text{Cl}_3$. Filled symbols mark MCE measurements, open symbols measurements of specific heat capacity. (b) Phase diagrams of $\text{CsNi}_{0.9}\text{Fe}_{0.1}\text{Cl}_3$ (solid line) and $\text{CsNi}_{0.98}\text{Fe}_{0.02}\text{Cl}_3$ (dotted line, determined using MCE from [7]), scaled by T_N and B_c , respectively. The shaded areas indicate the transition regions. For the U-F transition region, the boundaries are explicitly marked by begin and end of the decrease of the MCE as stated in the text.

Indeed $\text{CsNi}_{0.9}\text{Fe}_{0.1}\text{Cl}_3$, in a wide region of the P phase at higher magnetic fields, displays a negative MCE, *cf.* the 6 K-curve in Figure 5. The negative $\theta_H^* < 0$ and hence positive $\partial M/\partial T > 0$ are in agreement with the expected one-dimensional antiferromagnetic short-range order. At lowest magnetic fields in the P phase, the MCE becomes positive (Fig. 5).

In accordance with the considerations above, the MCE plateau at high fields and low temperatures which is identified as the U phase has positive sign, and in the fan phase a very small MCE is observed (Figs. 4, 5).

Somewhat unexpected is the observed change of sign of the MCE within the H phase, towards positive values at lowest temperatures (*cf.* the low-field region of the curves at 2 K and those at higher temperatures in Fig. 5 and the low-field low-temperature region in Fig. 4).

The resulting phase diagram is shown in Figure 7. It has the same topology as that of the compound doped with 2% Fe, demonstrating $0 < D/3J' < 1$. The fan phase extends to much lower temperatures as for 2% doping. The H-U transition takes place at a higher magnetic field, $B_c = (3.6 \pm 0.4)$ T at 2 K, *cf.* (2.3 ± 0.5) T at 3.6 K with 2% doping. The phase transition(s) at zero field, $T_{N1} = 5.3$ K and $T_{N2} = 5.1$ K, occur at a higher temperature than in the pure compound ($T_{N1} = 4.8$ K and $T_{N2} = 4.4$ K) and the 2% Fe-doped compound (4.64 K). Contrary to the 2% compound, the fan phase seems to have a finite width at zero field.

Some information on the intrachain exchange constant J is provided by the low-temperature part of the specific heat capacity. Antiferromagnetic Heisenberg chains with a linear dispersion of the magnetic excitations contribute linearly to the low-temperature specific heat capacity, $C/R = \kappa k_B T/|J|$ [11–15]. For spin 1, there is an excitation gap between the ground state and all magnetic excitations, the Haldane gap. Nevertheless, the calculations for finite chains demonstrate that the low-temperature specific heat capacity can still be approximated by a linear relation [13]. The predicted values of κ range from 0.108 to 0.28. Figure 8 presents the low-temperature specific heat capacity at zero field plotted as C/T vs. T^2 . A linear contribution for temperatures above T_N is obvious.

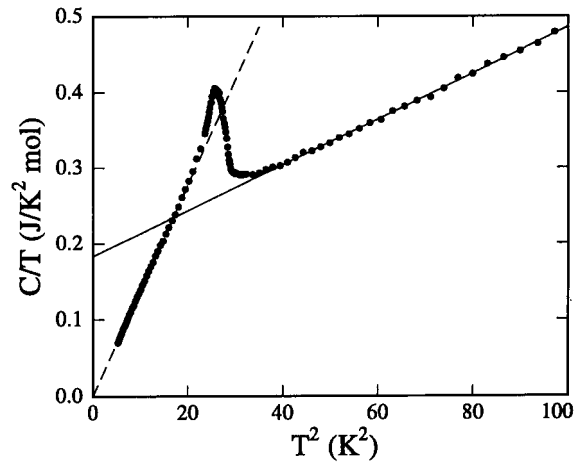


Fig. 8. Specific heat capacity of $\text{CsNi}_{0.9}\text{Fe}_{0.1}\text{Cl}_3$, measured with the quasi-adiabatic method, at zero field as C/T vs. T^2 . The full line is a fit of the temperature region above the phase transition to $C/T = a + bT^2$, the broken line is a fit of the low temperature region to $C/T = b'T^2$.

Fitting the function

$$C = aT + bT^3 \quad (5)$$

to the data above the phase transition yields $a = 0.183 \pm 0.005$ J/(mol K²) and $b = 3.02 \times 10^{-3} \pm 5 \times 10^{-5}$ J/(mol K⁴). The T -linear contribution to C can be observed in pure and 2% Fe²⁺ doped CsNiCl_3 as well. The data for CsNiCl_3 [17, 18] and $\text{CsNi}_{0.98}\text{Fe}_{0.02}\text{Cl}_3$ [19] coincide perfectly outside the critical region. From the data of Asano *et al.* [19] we extract $a = 0.179 \pm 0.005$ J/(mol K²). Hence, within the error bars, the linear contribution does not change between the pure, the 2% and the 10% Fe-doped compound. The resulting limits for the intrachain exchange of the 10% Fe-doped compound are $0.92 \leq J(10\% \text{ Fe})/J(\text{pure}) \leq 1.03$.

4 Discussion

The critical field $gB_c = 4S\sqrt{JD}$, the bounds of the effective J given by the linear part of the specific heat, and $J(\text{pure})/k_B = 16.6$ K imply an easy-plane anisotropy $D/k_B = (0.11 \pm 0.03)$ K for CsNi_{0.9}Fe_{0.1}Cl₃. This spread of D is remarkably small, considering the huge difference between the single ion anisotropies of Ni²⁺ and Fe²⁺, $D_{\text{Ni}}/k_B = -0.047$ K and $D_{\text{Fe}}/k_B = 14.8$ K. Moreover, the spread of the effective D does not increase from 2% to 10% doping.

The increase of the Néel temperature in spite of a rather large doping concentration is puzzling, one would rather expect a decrease of T_N due to the enhanced disorder. As $T_N \propto \sqrt{JJ'}$, the increased zero-field ordering temperature implies an increase of either the effective intrachain exchange or the interchain interaction (or both). However, the unchanged linear low-temperature part of the specific heat capacity confirms that J could have increased by at most 3% (error bar). With the limits of J given by the error bars of the determined specific heat slope, T_N implies an increase of the effective interchain interaction between 30% and 40%. With $J'(\text{pure})/k_B = 0.29$ K we obtain $J'(10\% \text{Fe})/k_B = (0.39 \pm 0.04)$ K. Possible origins for this increase of T_N and J' are discussed further below.

The values of D and J' yield $0.07 < D/3J' < 0.12$ which is still much smaller than 1. This should be compared to $0.02 < D/3J' < 0.07$ derived in the same way for the 2% doped compound. Hence the five times higher Fe²⁺ doping increases $D/3J'$ only by a factor of 2. With $D/3J' < 1$ the phase diagram of CsNi_{0.9}Fe_{0.1}Cl₃ like CsNi_{0.98}Fe_{0.02}Cl₃ is expected to be of the weak-anisotropy case, in agreement with our observation. The observed increase of $D/3J'$ reduces the relative extension of the umbrella phase which is expected to vanish entirely for $D/3J' = 1$. However, the extension of the fan phase at the cost of a part of the helix phase (*cf.* Fig. 7) and the extreme broadening of the U-F transition are surprising, in particular since the F-P transition remains remarkably sharp, and the H-U transition does not broaden with respect to the 2% compound. Of course, a general broadening of the phase transitions and a shift to lower temperatures can be expected in a doped material, as the doping may introduce disorder into the interchain and intrachain interactions. However, one would expect that the disorder affects all phase transitions. Therefore we need to understand why the P-F transition is not only shifted to higher temperatures than in pure CsNiCl₃, but also remains remarkably sharp and becomes even sharper with increasing field, while the U-F transition is extremely broadened. Table 1 summarizes the values for T_N , B_c , J , J' , D and the ratio $D/3J'$ for CsNi_{1-x}Fe_xCl₃ for $0 \leq x \leq 1$.

We will now consider several possible reasons for the broadening of a phase transition which seem to be near at hand, but can be shown to contradict some part of the observations. Finally we propose an explanation which is in agreement with all of our data, even with more subtle details.

At a first glance one might assume that the broadening of the U-F transition is caused by a large concentration gradient or inhomogeneities across the sample. Regions with larger $D/3J'$ would have a lower U-F transition temperature than regions with a smaller ratio. Variations of the concentration would lead to a spread of D as well as a spread of J' . The spread of D has been estimated above from the width of the H-U transition. The spread of J' should become visible at the P-F transition which is remarkably sharp. The specific heat data at 12 T provide an upper boundary of $\pm 2\%$ to such a spread of J' . Moreover, the influence of the spread of D and J' partly cancels on the ratio $D/3J'$, because regions with a high concentration of Fe²⁺ imply a high value of D as well as J' , since both, T_N and B_c increase with the concentration of Fe²⁺. In order to get a somewhat more quantitative estimate for the width of the U-F phase transition due to a concentration spread, we consider $T_c(D/3J')/T_c(0)$ at a given relative transition field, *e.g.* $2B_c$. $T_c(D/3J' = 0)$ coincides with the P-F transition, which in turn can be read of the phase diagram at 2% Fe, where no increase of $T_{\text{P-F}}$ was observed. Together with $T_c(D/3J' = 1) = 0$ and the two mean $T_c(D/3J')$ values of the two different concentrations we have four data points to estimate the dependence of $T_c(D/3J')/T_c(0)$ on $D/3J'$. Therefrom an expected transition width due to the spread of $D/3J'$ can be estimated. For the 2%-doped sample, the estimated spread of T_c 's corresponding to the spread of $D/3J'$ agrees within a few percent with the experimentally observed width (the shaded area in Fig. 7). For the 10% compound, however, the experimentally observed width of the U-F transition is 7 times larger than the estimated spread of T_c 's. This calls for another physical origin of the width of the U-F transition in the 10% Fe-doped compound.

Extreme broadening of phase transitions is known from defects which create random fields and random anisotropies, already at very low defect concentrations. Dramatic influences of doping, leading to random fields in an applied uniform field have been observed on the Ising antiferromagnet Fe_{1-x}Zn_xF₂ [25]. Random crystal field anisotropies lower and suppress the phase transitions in *e.g.* DyP_{1-x}V_xO₄ [26] very effectively, T_c drops by 30–50% for 10% defects.

Although we do not observe a drop of T_N but an increase upon doping, the possibility of random anisotropies in CsNi_{1-x}Fe_xCl₃ needs to be considered, because the crystal field anisotropy of Fe²⁺ is strong and easy-plane type, while that of Ni²⁺ is weak and Ising-type. The influence of random anisotropies should sensitively depend on the Fe²⁺ concentration (*cf.* DyP_{1-x}V_xO₄ [26]). The H-U phase transition is the one which is most sensitive to random anisotropy. This transition has a finite width, $B_c = (3.6 \pm 0.4)$ T. However, this width is still comparable to the width of a spin-flop transition in a pure material (*cf.* $B_c = (1.9 \pm 0.25)$ T in pure CsNiCl₃ [27]). Furthermore, the relative width of the H-U transition does not increase at all from 2% ($B_c = 2.3 \pm 0.5$ T) to 10% doping. This gives clear evidence, that the different crystal field anisotropies are effectively averaged by the strong one-dimensional

Table 1. Summary of the values found for $\text{CsNi}_{1-x}\text{Fe}_x\text{Cl}_3$ for $0 \leq x \leq 1$.

$\text{CsNi}_{1-x}\text{Fe}_x\text{Cl}_3$	x	T_N (K)	B_c (T)	J (K)	J' (K)	D (K)	$D/3J'$
	0	4.8, 4.4 ^a	1.9 ± 0.25^a	16.6 ± 0.4^a	0.29 ± 0.03^a	-0.033 ± 0.03^a	-0.038 ± 0.03^a
	0.02	4.64 ^b	2.3 ± 0.5^b	16.6 ± 0.8	0.30 ± 0.04	0.045 ± 0.02	0.05 ± 0.02
	0.1	5.3, 5.1	3.6 ± 0.4	16.6 ± 0.8	0.39 ± 0.04	0.11 ± 0.03	0.10 ± 0.02
	1	–	–	-7.1^a	1.9^a	14.8^a	2.57^a

^a Reference [1].^b Reference [7].

exchange interaction along the hexagonal axis, and random anisotropy behaviour is suppressed.

Next, we speculate, whether a single isolated Fe^{2+} , *i.e.* with only Ni^{2+} as next neighbours, can act as a random-field type defect through modified exchange interactions. The defect in search which causes the extreme U-F broadening of $\text{CsNi}_{0.9}\text{Fe}_{0.1}\text{Cl}_3$ should affect the P-F transition much less, and be consistent with the decreasing width of the P-F transition with increasing field. If the single Fe^{2+} acted as a random field type defect, already the phase transitions of the 2% Fe-doped sample should be lowered and broadened compared to the pure compound, and an increasing broadening with increasing field would be expected, contrary to the observation [7].

Nevertheless, we look into the exchange interactions in the neighbourhood of an isolated Fe^{2+} in more detail.

The intrachain exchange depends on bond lengths and bond angles, it is antiferromagnetic in CsNiCl_3 ($J/k_B = 16.6$ K), while that of CsFeCl_3 is ferromagnetic ($J/k_B = -7.1$ K). The Ni-Fe bond lengths and bond angles in the doped compound can be expected somewhere between the corresponding values in CsNiCl_3 and CsFeCl_3 . Hence it does not appear probable that the Ni-Fe intrachain exchange is *much stronger antiferromagnetic* than in CsNiCl_3 nor that it is *much stronger ferromagnetic* than in CsFeCl_3 . In any case, $J(\text{Ni-Fe})$ should be reflected in the effective J . For a crude estimate we may assume that $J(\text{Fe-Fe})$ and $J(\text{Ni-Ni})$ have the values of the respective pure compounds, and all interactions add up linearly to an effective J . Then the error bars of the effective J , determined from the linear part of $C(T)$, confine this crude estimate of $J(\text{Ni-Fe})$ to the interval $0.64 \leq J(\text{Ni-Fe})/J(\text{Ni-Ni}) \leq 1.25$. This implies an antiferromagnetic $J(\text{Ni-Fe})$.

A similar estimate based on the effective J' can be performed for the Ni-Fe interchain interaction $J'(\text{Ni-Fe})$, using $J'(\text{Ni-Ni})/k_B = 0.29$ K, $J'(\text{Fe-Fe})/k_B = 1.9$ K of the pure compounds. This yields $2.4 \leq J'(\text{Ni-Fe})/J'(\text{Ni-Ni}) \leq 2.9$, again an antiferromagnetic interaction.

With $J(\text{Ni-Fe})$ and $J'(\text{Ni-Fe})$ both antiferromagnetic as the corresponding Ni-Ni interactions, a single Fe^{2+} spin surrounded by Ni^{2+} at most generates small local distortions of the spin structure. With other words, an isolated Fe^{2+} leads to a weak magnetic bond dilution, but does not act as a random field type disturbance.

These considerations confirm that an isolated Fe^{2+} cannot be the defect which leads to the immense broadening of the U-F transition.

If we assume a statistical distribution of Fe^{2+} , the probability of Fe-Fe bonds cannot be neglected at 10% doping. We expect that two such Fe^{2+} neighbours are coupled as in CsFeCl_3 , *i.e.* ferromagnetically along the hexagonal axis and antiferromagnetically in the *ab*-plane. Hence a Fe-neighbour pair in the *ab*-plane will again not act as a random field type defect. To comprehend the influence of a Fe^{2+} neighbour pair along the one-dimensional *c*-axis, we first regard one single antiferromagnetic Ni-chain with one ferromagnetically coupled Fe^{2+} neighbour pair. The energy minimum of this chain is an arrangement where the Fe-pair constitutes a domain wall with respect to antiferromagnetic order along the chain. The staggered magnetization experiences a 180° phase slip at this domain wall, its orientation reverses. Such a chain cannot be incorporated into the H or U phase without a competition of interactions leading to entirely different preferred spin directions around the defect pair. This disturbance has a far-reaching influence, and constitutes a random-field type defect.

In the F phase, however, only the spin components along one axis are ordered. If the same chain with a one-dimensional domain wall defect is inserted, it can be incorporated by local adaptations of the expectation value of the staggered magnetization – the same Fe-pair defect does not introduce local changes of the preferred spin direction and hence does not act as a random field-type defect.

With the help of Figure 9 we wish to clarify the qualitative difference between a ferromagnetic Fe-pair defect in the F phase and the H and U phases. Figure 9a illustrates the spin orientation of the F structure in one hexagonal plane. At $c/2$ higher or lower, all spins are reversed. Two spins on a triangle are parallel. If one of these is flipped by 180° (gray arrow), its new orientation remains well adapted to the ordering direction of its neighbours, because the total energy can be minimized by length changes of the ordered moments. This scenario holds for all spins with “wrong” orientation in the entire reversed half-chain. If instead the third spin was flipped, so that three spins on a triangle become parallel (not shown), only one neighbour on this triangle needs to follow the flip in order to achieve an energy minimum similar to the previous one. A similar arrangement can be performed for the whole half-chain with the “false” orientation. In both cases, the resulting

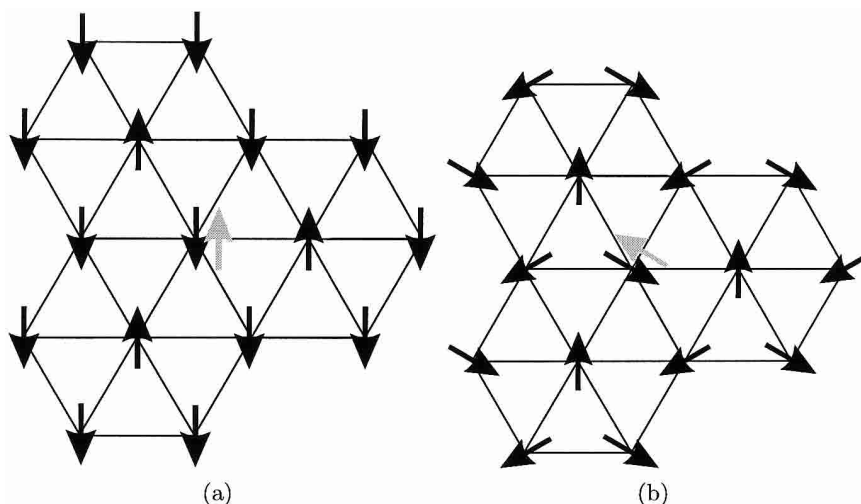


Fig. 9. Spin structures in the fan- (a) and the helixphase (b). The arrows indicate the ordering direction of the spins, respectively. The gray arrow represents a spin with a preference direction which is flipped by 180° with respect to the ordering direction given by the surrounding structure. Obviously, such a flipped spin is still reasonably well adapted in case of the fan phase, but not at all in the helix or umbrella phases.

structure satisfies the local antiferromagnetic interchain interactions on a triangle almost as well as without defect, but contains a line defect (consisting of one or two half-chains, respectively) with respect to the long-range order. Figure 9b illustrates the same hexagonal plane in the H phase. Obviously, the flipping of one spin requires a far-reaching rearrangement of the spin directions in order to achieve an energy minimum. The same problem occurs in the U phase, which can be regarded as a distorted 120° structure perpendicular to the easy plane (not shown).

We think that the easy incorporation of ferromagnetic Fe-pair defects into the F phase is responsible for the unexpected sharpness of the P-F transition even at 10% doping concentration. At the phase boundary to the U or H phases, however, these defects act as random field-type disturbances. Consequently, these phase boundaries become immensely broadened. Since the probability of such Fe-pairs is still very small at 2% doping, the width of the U-F transition is considerably smaller in that compound and does not exceed the width of the P-F transition.

The robustness of the F phase to these Fe-pair defects, which interfere severely with the order of the H and U phases, may not only cause the broadening of the U-F transition but also stabilize the F phase *versus* the H phase. It may produce the observed relative extension of the F phase at the cost of part of the H phase (Fig. 7) and even be responsible for the small finite zero-field width of the F phase. Nevertheless, alternative explanations should be considered for the zero-field width of the F phase. Of course pure CsNiCl_3 also performs two zero-field transitions (as in Fig. 1 left), but these are caused by the Ising anisotropy and occur at lower temperatures (4.4 K and 4.8 K). A superposition of Ising and easy-plane behaviour can be excluded, as only one transition, at 4.64 K, is observed in the 2% doped compound [7]. In several undoped ABX_3 compounds with easy-plane anisotropy, a finite width of the F phase at zero field is related to a dis-

tortion from the hexagonal symmetry, which leads to two different values of the antiferromagnetic interchain interactions on a triangle in the ab -plane. If CsNiCl_3 was close to such a structural distortion, local distortions could be promoted by doping. However, it is difficult to imagine, how a *random* distribution of impurities should lead to a *collective* distortion. The stability of the F phase with respect to ferromagnetic Fe-pair defects appears to be a much more natural explanation.

In fact, ferromagnetically coupled Fe-pairs in chain direction would also explain a number of other observations. We look again into the exchange interactions surrounding a Fe-pair along c . The interchain interaction J' in hexagonal ABX_3 compounds results from two almost equivalent exchange paths J'_1 and J'_2 (Fig. 10). Due to the strong intrachain exchange J along c , the spins are coupled firmly into an antiferromagnetic order in c -direction. As long as this antiferromagnetic order is perfect, the antiferromagnetic exchange J'_1 of one spin with a neighbour in the ab -plane will be almost cancelled by the antiferromagnetic exchange J'_2 to a spin in the same neighbouring chain, but $c/2$ higher or lower. This frustration leads to an almost vanishing effective $J' \ll J'_1, J'_2$ in the model Hamiltonian (1). With a ferromagnetic alignment of two neighbouring spins along c the frustration of the interchain exchange paths J'_1 and J'_2 to a common neighbour in an adjacent chain is removed and the effective J' raises to the order of $J'_1 + J'_2$. A dramatic increase of the effective interchain interaction J' had already been observed on CsNiCl_3 in high magnetic fields – ESR experiments [23] derive a 10 times larger interchain interaction from high-field experiments than neutron diffraction from zero-field data [24]. This virtual field dependence of J' is believed to result from these two almost equivalent interchain exchange paths which add their influence as soon as the magnetic field is strong enough to tilt the spins against the intrachain exchange. Note that the effective antiferromagnetic

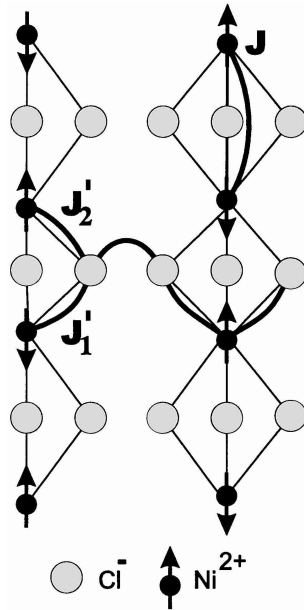


Fig. 10. Exchange paths in CsNiCl_3 .

interchain interaction J' in CsFeCl_3 (ferromagnetic along the chain) is seven times larger than in CsNiCl_3 which is antiferromagnetic along the chain [1], in complete agreement with these considerations. In this scenario, single isolated Fe^{2+} spins, coupled antiferromagnetically to their Ni-neighbours in c -direction, do not generate an increase of the effective interchain interaction. This implies an entirely homogeneous incorporation of isolated Fe-spins into the ordered structures, and explains why all phase transitions of the 2% compound remain so surprisingly sharp, with a Néel temperature which exactly coincides with the mean of the two transition temperatures in CsNiCl_3 .

Ferromagnetically coupled Fe-pairs in c -direction, however, remove the frustration of the surrounding J'_1, J'_2 paths. With 10% Fe^{2+} , about 2% Fe^{2+} occur in pairs along the chain. If these pairs are coupled ferromagnetically, about 4% of the interchain spin neighbour pairs experience an enhanced interchain interaction. Assuming a factor 10 enhancement of J' on the corresponding interchain bonds due to a removed J'_1, J'_2 frustration, the average effective antiferromagnetic interchain interaction J' indeed increases by 30–40%. With 2% Fe-doping, the same considerations lead to only 1% increase of the effective interchain interaction, because adjacent Fe-pairs along c are much less probable at lower concentration. The corresponding expected increase of T_N would be only 0.03 K, in agreement with the observation.

Moreover, the observed narrowing of the P-F transition towards higher magnetic fields is naturally explained in this scenario. (The width of the P-F transition decreases by a factor of 6 between $B = 0$ and 10 T in the 2% compound, down to $\sigma = 0.01$ K [7], and the 10% doped compound displays a similar narrowing, Fig. 2.) With increasing field, all spins align more and more parallel to the magnetic field. The spin arrangement around ferromagnetic defect pairs resembles more and more the

undisturbed structure. Hence the spread of effective J' 's, which depends on the spin alignment within the chains, is reduced with increasing field (and vanishes entirely at the saturation field) and correspondingly, the width of the transition temperature decreases with increasing field.

Finally we think that the existence of ferromagnetic Fe-spin pairs along the chain direction (coupled to the chain by a non-vanishing $J(\text{Ni-Fe})$) also explains the sign changes of the MCE which were observed in the P and the H phase.

In the P phase, where the temperature has overcome the interchain interaction, the compound may be regarded as an assembly of one-dimensional antiferromagnets. At all magnetic fields, the Fe-spin pair orients parallel to the magnetic field in order to minimize the magnetic energy of the pair. The small magnetic energy of the antiferromagnetic rest of the chain is optimized with the spins perpendicular to the field direction. At low fields, as long as the magnetic energy difference between parallel and perpendicular orientation of the antiferromagnetic chain part is smaller than the intrachain interaction $J(\text{Ni-Fe})$, all spins remain parallel and antiparallel to the field, and the magnetization is entirely due to the ferromagnetic Fe-spin pair. At higher magnetic fields, the antiferromagnetic chain pieces orient perpendicular to the field, and contribute to the magnetization by a small tilt into the field direction. This spin-flop like change of the orientation should affect $\partial M/\partial T$ from a ferromagnetic/paramagnetic to the usual behaviour of one-dimensional antiferromagnets, *i.e.* from a negative to a positive sign, corresponding to a positive sign of the MCE at low fields and a negative sign at higher fields. This is indeed the experimental observation. Our interpretation is further supported by the fact, that the sign change of the MCE at about 1.5 T is independent of temperature up to the highest measured temperatures.

In the H phase, with decreasing temperature, the spin configuration must adapt better and better to the Fe-pair defect in order to minimize the free energy. This leads to a random orientation of the spins of the ferromagnetic Fe^{2+} pairs at zero field. Near these pair defects the magnetization is not compensated. An increasing magnetic field then tries to turn the Fe-pair spins into the field direction, and the magnetization is at first mostly due to the ferromagnetic Fe-pair spins. Then, an increased temperature in the H phase only reduces the local uniform magnetization and again the compound shows a negative $\partial M/\partial T$ and a positive MCE like a paramagnet or ferromagnet.

We emphasize that all these considerations do not depend on a perfect parallel alignment of the Fe-spin neighbour pair in the ordered phases and are therefore independent of a precise knowledge of all exchange interactions. As long as neighbouring Fe-spins along the hexagonal axis experience a ferromagnetic exchange comparable to that in CsFeCl_3 and the intrachain exchange between Fe and Ni is not zero but at least comparable to the interchain interaction, the qualitative features are expected to remain the same.

5 Conclusion

We investigated CsNi_{0.9}Fe_{0.1}Cl₃ by specific heat capacity and magnetocaloric effect measurements. The combination of the two techniques, which can be performed with essentially the same equipment, allows the determination of the complete *B-T* phase diagram. Three very surprising results, the very different degree of broadening of the phase boundaries, the decreasing width of the P-F phase boundary with increasing field and the increase of the P-F transition temperature in spite of a large doping concentration can be explained by the existence of ferromagnetically coupled Fe-spin pairs along the chain direction and the consequent removal of frustration in the interchain interactions. We emphasize that our findings cannot be explained by a simple concentration gradient across the sample. The ferromagnetic Fe-pair defects also seem to be responsible for more subtle details in the caloric experiments (like sign changes of the magnetocaloric effect within one phase) and hence yield a consistent picture. In this scenario, only Fe-pairs along the *c*-direction limit the ordering process, while isolated Fe-spins are homogeneously incorporated into the ordered structures. This explains on a microscopic basis, why the tuning of the anisotropy with Fe-impurities is so successful at low doping concentrations. Since Fe-pairs along the hexagonal axis represent random field type defects in two of the ordered phases, it is the number of these pair defects which limits the modeling of the anisotropy *via* doping with Fe²⁺. Eventually the phase transitions will wash out entirely. Hence our experiments and analysis reveal and explain the potentials and limitations of a modelling of the anisotropy of CsNiCl₃ *via* Fe²⁺ impurities.

We thank T. Asano and Y. Ajiro for supplying the sample. The work has been funded by the German Bundesministerium für Bildung und Forschung, project KN5SAA-03.

References

- M.F. Collins, O.A. Petrenko, *Can. J. Phys.* **75**, 605 (1997).
- J. Takeushi, T. Wada, I. Hiromitsu, T. Ito, *Sol. State Commun.* **87**, 899 (1993).
- E. Rastelli, A. Tassi, *Phys. Rev. B* **50**, 16475 (1994).
- S.I. Abarzhi, A.V. Chubukov, *J. Phys. Cond. Matt.* **2**, 9221 (1990).
- M.L. Plumer, A. Caillé, *Phys. Rev. B* **39**, 4489 (1989).
- M. Winkelmann, R. Schneider, M. Enderle, T. Asano, Y. Ajiro, M. Steiner, *J. Phys. Cond. Matt.* **9**, 703 (1997).
- K. Kiefer, K. Knorr, M. Enderle, *J. Magn. Magn. Mater.* (accepted for publication).
- K. Kiefer, Master's thesis, Universität des Saarlandes (1997).
- J.C. Lasjaunias, B. Picot, A. Ravex, D. Thoulouze, M. Vandorpe, *Cryogenics* **17**, 111 (1977).
- B. Fischer, J. Hoffmann, H.G. Kahle, W. Paul, *J. Magn. Magn. Mater.* **94**, 79 (1991).
- R. Kubo, *Phys. Rev.* **87**, 568 (1952).
- J.C. Bonner, M.E. Fisher, *Phys. Rev A* **135**, 640 (1964).
- H.W. Blöte, *Physica B* **79**, 427 (1975).
- T. de Neef, *Phys. Rev. B* **13**, 4141 (1976).
- H. Igarashi, *J. Phys. Soc. Jpn* **54**, 516 (1985).
- D. Moses, H. Shechter, E. Ehrenfreund, J. Makovsky, *J. Phys. C* **10**, 433 (1977).
- S.J. Collocott, J.A. Rayne, *J. Appl. Phys.* **61**, 4404 (1987).
- D. Beckmann, J. Wosnitzer, H.v. Löhneysen, D. Visser, *Phys. Rev. Lett.* **71**, 2829 (1993).
- T. Asano, Y. Ajiro, M. Mekata, K. Kamashima, T. Goto, H. Aruga Katori, K. Katsumata, *J. Magn. Magn. Mater.* **177-181**, 640 (1998).
- M. Enderle, Ph.D. thesis, Johannes Gutenberg Universität Mainz, Germany (1993).
- T. Goto, T. Inami, Y. Ajiro, *J. Phys. Soc. Jpn* **59**, 2328 (1990).
- H. Tanaka, H. Nakano, S. Matsuo, *J. Phys. Soc. Jpn* **63**, 3169 (1994).
- W. Palme, H. Krieglstein, O. Born, A. Chennaoui, B. Lüthi, *Z. Phys. B* **92**, 1 (1993).
- K. Kakurai, M. Steiner, R. Pynn, J.K. Kjems, *J. Phys. Cond. Matt.* **3**, 715 (1991).
- D.P. Belanger, *Phase Transitions* **11**, 53 (1988).
- P. Kettler, M. Steiner, H. Dachs, R. Germer, B. Wanklyn, *Phys. Rev. Lett.* **47**, 1329 (1981).
- P.B. Johnson, J.A. Rayne, S.A. Friedberg, *J. Appl. Phys.* **50**, 1853 (1979); H. Weber, D. Beckmann, J. Wosnitzer, H.v. Löhneysen, D. Visser, *Int. J. Mod. Phys.* **9**, 1387 (1995).